bioRxiv preprint doi: https://doi.org/10.1101/2021.01.08.425793; this version posted March 18, 2021. The copyright holder for this preprint (which was not certified by peer review) is the author/funder, who has granted bioRxiv a license to display the preprint in perpetuity. It is made available under aCC-BY-NC 4.0 International license.

Supplementary Figures

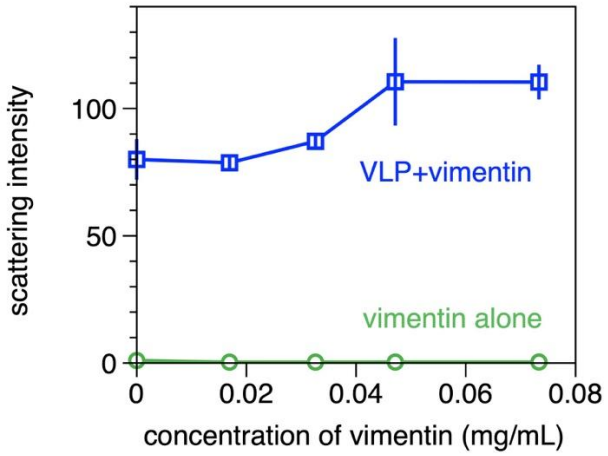

SI Fig. 1. The scattering intensity of the viral parties was much larger than that of the added vimentin and was increased after adding vimentin.

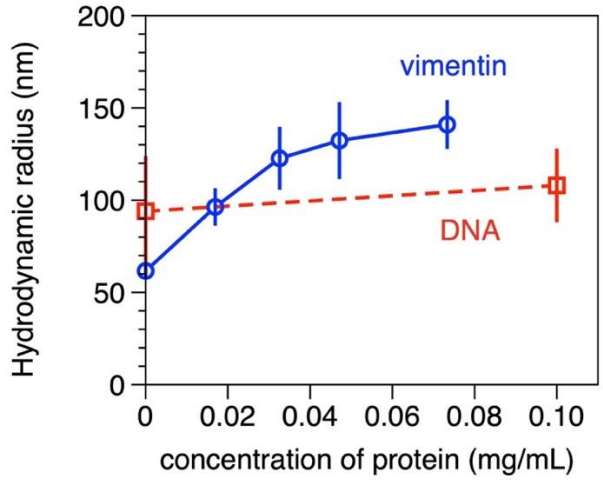

SI Fig. 2. Dynamic light scattering data showing the relative increase of pseudovirion particles with addition of either vimentin or DNA. Addition of vimentin increases relative size of the particles whereas DNA does not.

bioRxiv preprint doi: https://doi.org/10.1101/2021.01.08.425793; this version posted March 18, 2021. The copyright holder for this preprint (which was not certified by peer review) is the author/funder, who has granted bioRxiv a license to display the preprint in perpetuity. It is made available under aCC-BY-NC 4.0 International license.

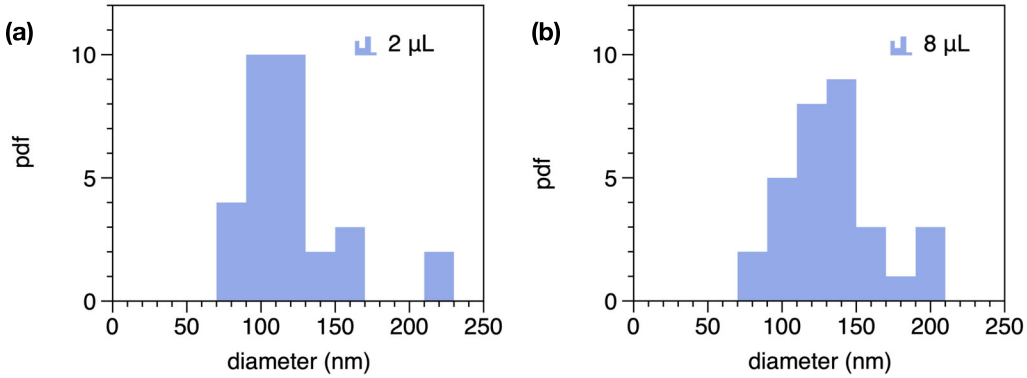

SI Fig. 4. The probability distribution function of particle diameter for SARS-CoV-2 pseudovirus samples after the addition of either (a) 2 µL or (b) 8 µL of 10 mg/mL DNA. Particle sizes were measured by atomic force microscopy.

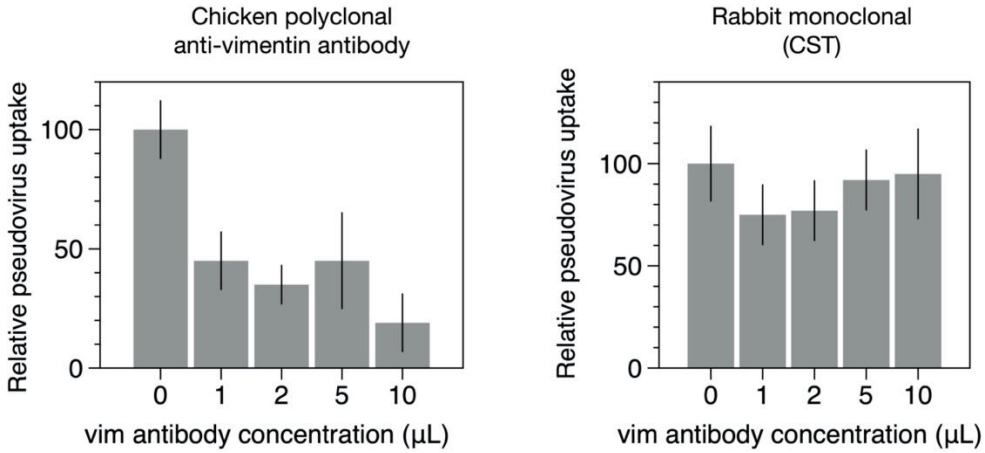

SI Fig. 5. Results from the anti-vimentin rabbit monoclonal antibody from Cell Signaling Technologies does not block uptakes of SARS-CoV-2 pseudovirus in HEK 293T-hsACE2 cells. Error bars represent mean ± standard deviation.

bioRxiv preprint doi: https://doi.org/10.1101/2021.01.08.425793; this version posted March 18, 2021. The copyright holder for this preprint (which was not certified by peer review) is the author/funder, who has granted bioRxiv a license to display the preprint in perpetuity. It is made available under aCC-BY-NC 4.0 International license.

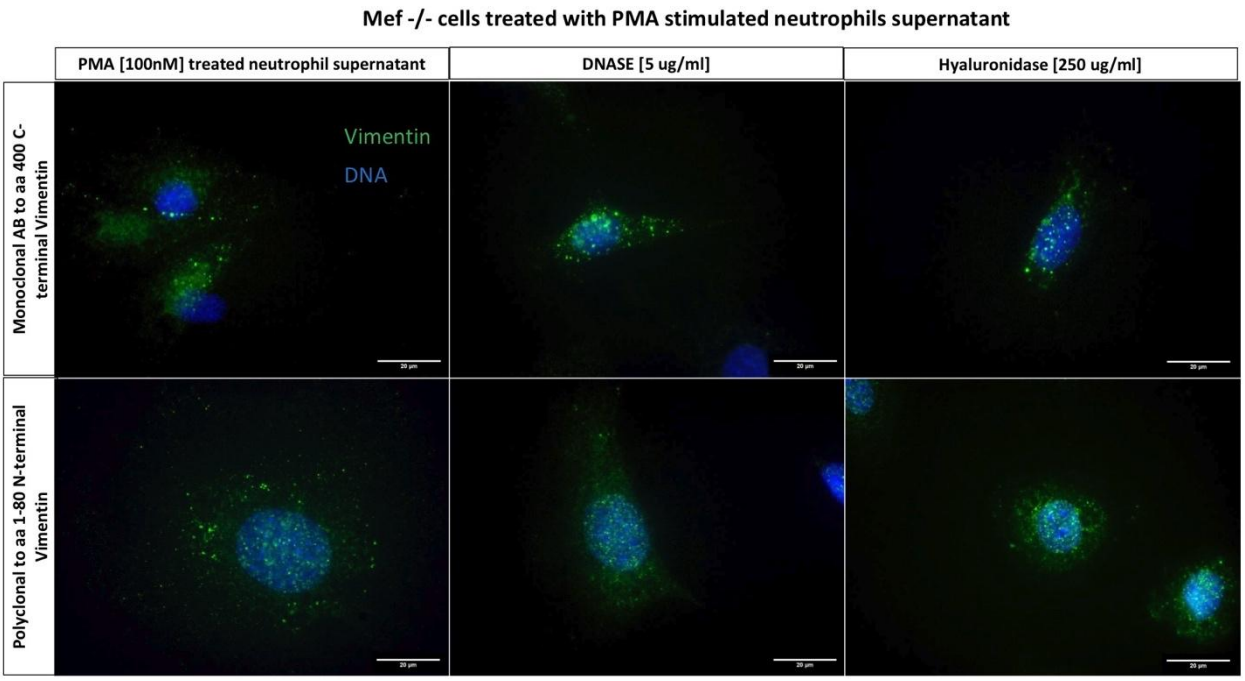

SI Fig. 6. Immunofluorescence images indicating presence of cell surface vimentin on vim -/- mEF after exposure to PMA-stimulated neutrophil supernatant. Neither DNASE or hyaluronidase treatment alters the presence of cell surface vimentin.

bioRxiv preprint doi: https://doi.org/10.1101/2021.01.08.425793; this version posted March 18, 2021. The copyright holder for this preprint (which was not certified by peer review) is the author/funder, who has granted bioRxiv a license to display the preprint in perpetuity. It is made available under aCC-BY-NC 4.0 International license.

"Extracellular vimentin as a target against SARS-CoV-2 host cell invasion": Supplemental Information

A. Modeling cell surface vimentin, SARS-CoV-2 and cell-membrane interactions

To test the notion that extracellular vimentin bound to the cell membrane can initiate endocytosis of the SARS2 virus, we developed a multiscale, coarse-grained molecular dynamics-based computational model. The model consists of a cell membrane, extracellular vimentin (ECV), the angiotensin-converting enzyme 2 (ACE2), and a virus containing spike proteins.

The cell membrane is modeled as a self-avoiding, tethered sheet with fixed connectivity as shown in Fig. [1]. It is a network of equilateral triangles consisting of particles as N nodes and tethers to connect them. The two-dimensional sheet is embedded in three-dimensional Euclidean space. We introduce self-avoidance to the system by satisfying the condition $l_o/\sigma_o < \sqrt{3}$, where l_o is the edge length of a triangle in the mesh and σ_o is the diameter of a particle [1]. Stretchability of the membrane is encoded in nearest-neighbor harmonic springs with the energy

$$E_S^{Mem} = \frac{K_{NN}^{Mem}}{2} \sum_{<ij>} \left(r_{ij} - l_o\right)^2, \tag{1}$$

with spring constant K_{NN}^{Mem} and $< ij >$ represents all nearest-neighbor nodes i and j. We also have an explicit bending rigidity modeled by adding another harmonic spring between every second nearest neighbor of each node [2, 3] having energy

$$E_B^{Mem} = \frac{K_{SNN}^{Mem}}{2} \sum_{<<ik>>} \left(r_{ik} - \sqrt{3} l_o\right)^2, \tag{2}$$

with $<< ik >>$ denoting all second-nearest neighbors. Spring constant K_{SNN}^{Mem} can be converted to a bending rigidity .

Given the experimental findings of non-filamentous extracellular vimentin bound to the cell membrane, we focus on extracellular vimentin tetramers [4]. The extracellular vimentin tetramers are represented as semiflexible filaments, containing both springs between two consecutive monomers with spring constant, K_{NN}^{Vim}, and angular springs between three consecutive monomers to capture the bending rigidity with angular spring constant, K_{Ang}^{Vim}. The energy for each monomer triplet is, therefore,

$$E_{Ang}^{Vim} = \frac{K_{Ang}^{Vim}}{2} \left(\cos(\theta_{lmn}) - 1\right)^2, \tag{3}$$

where l, m, n denote three consecutive monomers along the filament. For simplicity, we have assumed the ACE2 receptor is the same length as the vimentin tetramers and is also a semiflexible filament with corresponding two-body springs and angular springs, K_{NN}^{ACE2} and K_{Ang}^{ACE2}, respectively. The ACE2 receptor is stiffer than vimentin and provides stability during the wrapping process. Both the vimentin tetramers and the ACE2 receptor are also connected with the membrane via springs as shown in Fig. [2] with the same two-body spring constant, which gives them the freedom to bend at any angle with respect to the membrane. We place extracellular vimentin randomly on the membrane with coverage ϕ_{Vim}, whereas ACE2 is located at the center of the membrane. The extracellular vimentin now becomes cell-surface vimentin.

The virus is modeled as a deformable shell with spikes. The shell is constructed as a Fibonacci sphere, where particles/monomers are placed on the sphere in a spiral. We use a Delaunay triangulation to find triangles amongst the particles and their corresponding edges. These particles are also connected via nearest-neighbor harmonic springs each with spring constant, K_{NN}^{Virus} to arrive at a tethered spherical membrane with fixed connectivity. Spike proteins are homogenously placed on the shell surface as shown in Fig. [3]. The spike protein filaments also have harmonic spring potential between two consecutive monomers with spring constant K_{NN}^{Spike}. Their bending rigidity is also coded via 3-body, or angular, spring with spring constant, K_{Ang}^{Spike}. The spike protein filaments can take any angle with respect to the virus [5, 6].

To take into account excluded volume interactions, we implement a soft-core repulsion spring between all monomers with no other interactions via energy

$$V_{Repel} = \begin{cases} \frac{K_{Repel}}{2} \left(r_{ij} - \sigma_o\right)^2 & r \leqslant \sigma_o \\ 0 & r > \sigma_o. \end{cases} \tag{4}$$

bioRxiv preprint doi: https://doi.org/10.1101/2021.01.08.425793; this version posted March 18, 2021. The copyright holder for this preprint (which was not certified by peer review) is the author/funder, who has granted bioRxiv a license to display the preprint in perpetuity. It is made available under aCC-BY-NC 4.0 International license.

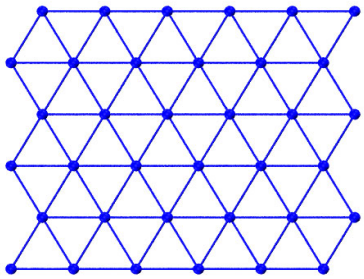

FIG. 1. *Tethered membrane as a cell membrane.* Blue particles denote the nodes of the triagular mesh and blue lines denote the tethers.

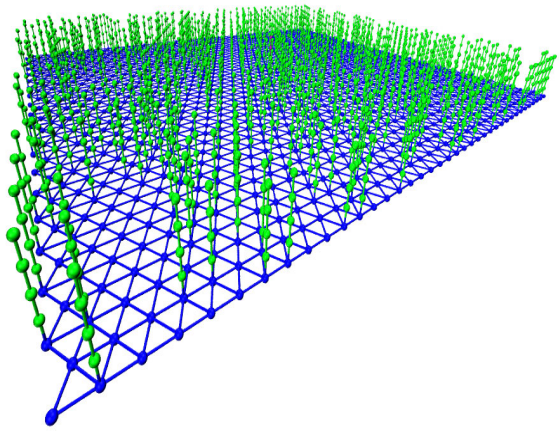

FIG. 2. *Cell membrane with bound extracellular vimentin.* Extracellular vimentin (ECV) tetramers are denoted in green. ECV tetramers are randomly attached to the cell surface to become cell surface vimentin. The coverage of extracellular vimentin depicted here is $\phi_{Vim} = 0.4$, i.e., 40 percent of the membrane nodes have bound ECV.

As for other interactions, the spike-ACE2 interaction is modeled as a stiff harmonic spring between the two filament ends with spring constant $K_{NN}^{ACE2-Spike}$ since ACE2 has a high affinity to the spike protein [7, 8]. Additionally, there is an attractive Lennard-Jones potential between the spike protein and the cell surface vimentin with a higher cut-off at $2\sigma_o$ as given by

$$V_{LJ} = \begin{cases} 4\epsilon \left[\left(\frac{\sigma_o}{r_{ij}}\right)^{12} - \left(\frac{\sigma_o}{r_{ij}}\right)^{6} \right] & r \leqslant 2\sigma_o \\ 0 & r > 2\sigma_o. \end{cases} \tag{5}$$

To convert our simulation units to biological units, we use 1 simulation unit length $= 10\,nm$, 1 unit simulation time$= 10^{-3}\,s$ and 1 unit force $= 10^{-1}\,pN$. From these scales, we can define all the parameters in biological units. The diameter of the virus is $100\,nm$, which is very similar to our own DLS measurements and similar to SARS2 [9–11]. The size of the virus is small compared to the size of the cell, typically $\sim 20\ \mu m$ in diameter, which is about 200 times bigger than the virus. Thus, during endocytosis, the virus is interacting with a small patch of the cell membrane. Hence, we simulated a tethered sheet of $length \times width = 55\,nm \times 480.6\,nm$, which is a small surface area of the cell

bioRxiv preprint doi: https://doi.org/10.1101/2021.01.08.425793; this version posted March 18, 2021. The copyright holder for this preprint (which was not certified by peer review) is the author/funder, who has granted bioRxiv a license to display the preprint in perpetuity. It is made available under aCC-BY-NC 4.0 International license.

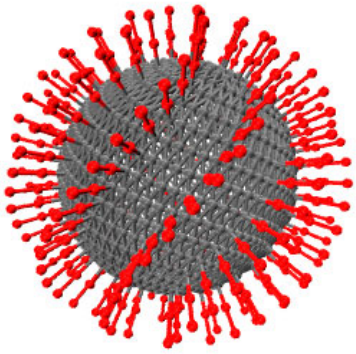

FIG. 3. *SARS2 virus.* Spike proteins are placed homogeneously on the surface of the virus.

membrane. This cell surface is covered with cell surface vimentin tetramers of length $40\,nm$, which is slightly smaller than the more typical $60-90\,nm$. We vary the density of the extracellular vimentin (ECV) to quantify its effect on viral uptake. The number of spike proteins on the viral surface can be different based on virus size [12]. We consider 200 spikes[9, 11, 13, 14] on the virus each of length $20\,nm$ [5, 9, 15] and diameter $10\,nm$ [11], to which ECV can attach. The bending rigidity of cell membrane is approximately $40k_BT$ based on the scales we have defined. Finally, each simulation was run for 10^8 simulation time units, which corresponds to $50\,s$ with recording trajectory data every $25\,ms$. See Table 1 for the parameters used in the simulations.

For each set of parameters, 10 realizations were computed and used to compute average quantities of the fraction of spike proteins bound to ECV, and the degree of wrapping by the cell membrane, as defined in the Methods section of the manuscript. All computed quantities indicate the extent of endocytosis, or wrapping, of the virus by ECV.

bioRxiv preprint doi: https://doi.org/10.1101/2021.01.08.425793; this version posted March 18, 2021. The copyright holder for this preprint (which was not certified by peer review) is the author/funder, who has granted bioRxiv a license to display the preprint in perpetuity. It is made available under aCC-BY-NC 4.0 International license.

Parameters	Value	Reference
K_{NN}^{Mem}	$1\,pN/nm$	[16] [17]
K_{SNN}^{Mem}	$0.1\,pN/nm$	[18] [19]
K_{NN}^{Virus}	$50\,pN/nm$	SARS Cov-2[20], Brone mosaic virus [21] ,influenza virus[22] , Human Adenovirus [23] Deformable NP[24]
K_{NN}^{Spike}	$0.1\,pN/nm$	[25]
K_{NN}^{Vim}	$1\,pN/nm$	[26]
K_{NN}^{ACE2}	$5\,pN/nm$	-
$K_{NN}^{ACE2-Spike}$	$5\,pN/nm$	[27]
K_{Ang}^{ACE2}	$500k_BT$	-
K_{Ang}^{Vim}	$100k_BT$	-
K_{Ang}^{Spike}	$100k_BT$	-
ϵ	$10k_BT$	-
K_{Repel}	$1\,pN/nm$	-

TABLE I. Table of parameters used unless otherwise specified.

[1] Y. Kantor, M. Kardar, and D. R. Nelson, Physical Review Letters **57**, 791 (1986).
[2] D. Boal, E. Levinson, D. Liu, and M. Plischke, Physical Review A **40**, 3292 (1989).
[3] M. Plischke and D. Boal, Physical Review A **38**, 4943 (1988).
[4] B. Hwang and H. Ise, Genes to Cells **25**, 413 (2020).
[5] H. Yao, Y. Song, Y. Chen, N. Wu, J. Xu, C. Sun, J. Zhang, T. Weng, Z. Zhang, Z. Wu, L. Cheng, D. Shi, X. Lu, J. Lei, M. Crispin, Y. Shi, L. Li, and S. Li, Cell **183**, 730 (2020).
[6] B. Turoová, M. Sikora, C. Schürmann, W. J. Hagen, S. Welsch, F. E. Blanc, S. von Bülow, M. Gecht, K. Bagola, C. Hörner, G. van Zandbergen, J. Landry, N. T. D. de Azevedo, S. Mosalaganti, A. Schwarz, R. Covino, M. D. Mühlebach, G. Hummer, J. Krijnse Locker, and M. Beck, Science (New York, N.Y.) **370**, 203 (2020).
[7] D. Wrapp, N. Wang, K. S. Corbett, J. A. Goldsmith, C. L. Hsieh, O. Abiona, B. S. Graham, and J. S. McLellan, Science **367**, 1260 (2020).
[8] E. S. Brielle, D. Schneidman-Duhovny, and M. Linial, Viruses **12** (2020).
[9] S. Klein, M. Cortese, S. L. Winter, M. Wachsmuth-Melm, C. J. Neufeldt, B. Cerikan, M. L. Stanifer, S. Boulant, R. Bartenschlager, and P. Chlanda, Nature Communications **11**, 1 (2020).
[10] N. Zhu, D. Zhang, W. Wang, X. Li, B. Yang, J. Song, X. Zhao, B. Huang, W. Shi, R. Lu, P. Niu, F. Zhan, X. Ma, D. Wang, W. Xu, G. Wu, G. F. Gao, and W. Tan, New England Journal of Medicine **382**, 727 (2020).
[11] B. W. Neuman, B. D. Adair, C. Yoshioka, J. D. Quispe, G. Orca, P. Kuhn, R. A. Milligan, M. Yeager, and M. J. Buchmeier, Journal of Virology **80**, 7918 (2006).
[12] B. W. Neuman, G. Kiss, A. H. Kunding, D. Bhella, M. F. Baksh, S. Connelly, B. Droese, J. P. Klaus, S. Makino, S. G. Sawicki, S. G. Siddell, D. G. Stamou, I. A. Wilson, P. Kuhn, and M. J. Buchmeier, Journal of Structural Biology **174**, 11 (2011).
[13] M. Ponga, Scientific Reports **10**, 2 (2020).
[14] Z. Ke, J. Oton, K. Qu, M. Cortese, V. Zila, L. McKeane, T. Nakane, J. Zivanov, C. J. Neufeldt, B. Cerikan, J. M. Lu,

bioRxiv preprint doi: https://doi.org/10.1101/2021.01.08.425793; this version posted March 18, 2021. The copyright holder for this preprint (which was not certified by peer review) is the author/funder, who has granted bioRxiv a license to display the preprint in perpetuity. It is made available under aCC-BY-NC 4.0 International license.

J. Peukes, X. Xiong, H. G. Kräusslich, S. H. Scheres, R. Bartenschlager, and J. A. Briggs, Nature **588** (2020).
[15] D. Cavanagh, Coronaviruses with Special Emphasis on First Insights Concerning SARS , 1 (2005).
[16] C. E. Morris and U. Homann, Journal of Membrane Biology **179**, 79 (2001).
[17] P. Chugh, A. G. Clark, M. B. Smith, D. A. Cassani, K. Dierkes, A. Ragab, P. P. Roux, G. Charras, G. Salbreux, and E. K. Paluch, Nature Cell Biology **19**, 689 (2017).
[18] J. Eid, H. Razmazma, A. Jraij, A. Ebrahimi, and L. Monticelli, Journal of Physical Chemistry B **124**, 6299 (2020).
[19] R. Dimova, Advances in Colloid and Interface Science **208**, 225 (2014).
[20] B. Kiss, Z. Kis, B. Pályi, and M. S. Z. Kellermayer, bioRxiv , 2020.09.17.302380 (2020).
[21] C. Zeng, M. Hernando-Pérez, B. Dragnea, X. Ma, P. Van Der Schoot, and R. Zandi, Physical Review Letters **119**, 1 (2017).
[22] I. A. Schaap, F. Eghiaia, A. Des George, and C. Veigel, Journal of Biological Chemistry **287**, 41078 (2012).
[23] P. J. de Pablo and I. A. T. Schaap, in *Advances in Experimental Medicine and Biology*, Vol. 1140 (2019) pp. 159–179.
[24] L. Chen, X. Li, Y. Zhang, T. Chen, S. Xiao, and H. Liang, Nanoscale **10**, 11969 (2018).
[25] R. A. Moreira, M. Chwastyk, J. L. Baker, H. V. Guzman, and A. B. Poma, Nanoscale **12**, 16409 (2020).
[26] Z. Qin, L. Kreplak, and M. J. Buehler, PLoS ONE **4**, e7294 (2009).
[27] C. Bai and A. Warshel, Journal of Physical Chemistry B **124**, 5907 (2020).